mathematics

Article

The Impact of Thermal Radiation on Mixed Convective Unsteady Nanofluid Flow in a Revolving Vertical Cone

Shweta Mishra [1], Hiranmoy Mondal [1], Ramandeep Behl [2,*] and Mehdi Salimi [3]

1 Department of Applied Mathematics, Maulana Abul Kalam Azad University of Technology, Kolkata 713212, West Bengal, India; shweta.mishra@makautwb.ac.in (S.M.); hiranmoy.mondal@makautwb.ac.in (H.M.)
2 Mathematical Modelling and Applied Computation Research Group (MMAC), Department of Mathematics, King Abdulaziz University, Jeddah 21589, Saudi Arabia
3 Decisions Lab, DiGiES, Mediterranea University of Reggio Calabria, 89125 Reggio Calabria, Italy; mehdi.salimi@unirc.it
* Correspondence: rlal@kau.edu.sa

Abstract: This study investigates the effects of an unsteady mixed convection nanofluid flow in a rotating vertical cone submerged in spinning nanofluid. Our analysis considered the impacts of heat flux, chemical reactions, and thermal radiation, with the thermal and concentration Biot numbers serving as constraints at the boundary. The governing unsteady and coupled partial differential equations were solved through appropriate similarity transformations, addressing the nonlinear terms inherent in these equations. The spectral quasi-linearisation method (SQLM) was employed to solve the higher-order nonlinear differential equations. This study elucidates and assesses the impact of diverse physical constraints and parameters through the use of graphical representations. Notably, the temperature distribution of the liquefied substance was intensified as the thermal and solutal Biot numbers increased.

Keywords: unsteady mixed convection; chemical reaction; heat flux; vertical cone; thermal radiation; Biot numbers

MSC: 35Q30; 76M55; 65B15; 34A12

check for updates

Citation: Mishra, S.; Mondal, H.; Behl, R.; Salimi, M. The Impact of Thermal Radiation on Mixed Convective Unsteady Nanofluid Flow in a Revolving Vertical Cone. *Mathematics* **2024**, *12*, 349. https://doi.org/10.3390/math12020349

Academic Editor: Vasily Novozhilov

Received: 6 December 2023
Revised: 10 January 2024
Accepted: 15 January 2024
Published: 22 January 2024

1. Introduction

The adoption of vertically oriented rotating cones with nanofluids in motion has garnered interest across diverse industries and engineering disciplines, including turbine design, flight path estimation, and missile technology. The problem of unsteady nanofluid flow in a revolving vertical cone has drawn interest because of its application within many engineering problems, boundary layer control in aerodynamics, geophysics (the cooling towers, for example), astrophysics, and nuclear reactor cooling. As an axisymmetric shape moves within a defined stream flow, the centrifugal force radially propels the fluid near the surface in an outward direction. Consequently, the axial velocity of the fluid in proximity to the spinning object intensifies, leading to an augmented convective heat transfer between the object and the fluid. This phenomenon has found practical applications in relation to enhancing heat transfer within various systems.

Nanofluids have piqued the curiosity of many due to their unique features, as they are beneficial in glass blowing, thermal treatment for cancer, extrusion in elastics and polymers, cooling and air conditioning, and micro-forming, among other industrial processes. The term "nanofluid" was first introduced by Choi to describe a mixture of liquid and nano-sized particles. Ali et al. [1] investigated the magnetohydrodynamics (MHD) convective free-forced Hiemenz liquid flow past an absorbent medium and solved the governing equations using the finite difference iterative method. Meanwhile, Abolbashari et al. [2]

investigated the Casson fluid flow by considering entropy generation and concluded that reducing the Casson parameter enhances entropy. Meanwhile, Mishra et al. [3] discussed the effects of heat generation on couple stress nanofluids.

When mass transfer and heat transfer happen simultaneously in a continuous fluid, the driving potential and fluxes have a more complicated relationship. In addition to composition gradients, temperature gradients can also result in an energy flux. In manufacturing, simply using unrestricted enforced convection is not enough to diffuse acceptable heat energy. The mixed convection on the fluid stream is very significant. A study conducted by Kalidasan et al. [4] explored convective H_2O-based alumina nanofluid flow placed in a cubical bar and found that chemical reactions play a significant role in nanofluid flow. G. Manjunatha [5] examined the flow of Jeffery-nanoscale fluid within the peristaltic channel and observed that the fluid temperature profile improves with the growth of Biot numbers. Dhlamini et al. [6] investigated the impacts of activation energy on nanofluid flow with large-scale chemical reactions and concluded that velocity and concentration profiles significantly improve the chemical reaction. However, for temperature, the profile showed the opposite behaviour as it decreased for a higher chemical reaction rate. The radiative heat flux of hydro-magnetic nanofluid on Williamson fluid was studied by Mishra et al. [7], while Dhlamini et al. [8] studied the impact of thermal conduction and non-uniform viscous force on nanofluid flow in the presence of couple stress and found that high rates of heat conduction and couple stress result in more heat and mass transportation. Awad Musa et al. and Konda [9,10] studied the melting heat mass transfer effects of thermal radiation on hydro-dynamic nanofluid flow and found that the temperature profile grows with the magnetic field effect. Muhammad and Abbas [11] studied heat and mass transportation on Maxwell-type nanofluid. Thumma et al. [12] investigated the effects of joule and viscous dissipation on Powell–Eyring nanofluid flow passing over an extended lamina.

Numerous studies have explored the impact of viscous dissipation on convective heat redistribution in porous media. A specific subset of researchers [13,14] has delved into examining the effects of heat mass transmission on natural convection. This investigation considers non-Darcy permeability in a submerged perpendicular cone and various parameters in a non-Newtonian fluid.

Examining heat and mass transfer with convective boundary conditions holds significance in industries such as temperature exchangers, gas turbines, and atomic reactors. Heat is transferred from the boundary surface to the convective fluid which possesses heat capacity, giving rise to the establishment of a convective heat transmission constant, known as the thermal Biot number.

Nanofluids have found numerous applications in biomedical sciences, including the labeling of cancerous tissues, the imaging of magnetic resonance known as MRI, nano-cryosurgery, nano-drug delivery, and other medicinal purposes studied by Bhatti et al. [15]. Several academics have observed the impact of viscous dissipation on convective nanofluid flow via vertical surface. Additionally, various researchers have numerically investigated mixed convection nanofluid streams with plates in an upward direction using different parameters (see [16–21]).

Thermal radiation plays a crucial role in the transfer of heat and flow in the presence of a magnetic field. Its significance extends to various fields such as aerospace science, solar power, the production of electricity, and glasses. The requirement for energy in different sectors has motivated scientists to work on controlling and managing heat. Rashidi et al. [22] discussed the impact of thermal radiation on viscoelastic fluids, while Makinde and Ogulu [23] numerically discussed the thermal radiation's impact on unrestricted convective flow within the magnetic field. Hayat et al. [24] examined the effect of ohmic heating on the radiative surface in third-grade fluids. Various investigators have also analysed thermal radiation using other parameters (see [25,26]).

The key point of this study is to see the effects of Biot numbers and thermalradiation on the revolving vertical cone with the spectral quasi-linearisation method (SQLM), which has not been explained yet. The primary objective of this investigation was to explore the influence of unsteady mixed convection nanofluid flow in a vertically rotating cone, incorporating thermal radiation and chemical reactions. Additionally, we considered the effects of solutal and thermal Biot numbers at boundary conditions. The angular velocity of the cone experienced variations due to both its rotation and that of the nanofluid, leading to fluctuations in the nanofluid flow field. Our proposed model involved an energy equation encompassing nanofluid and thermal radiation, and a concentration equation accounting for chemical reactions, resulting in highly nonlinear coupled partial differential equations. These equations were transformed into conventional difference equations (ODEs) through significant similarity transformations. Statistical analysis, employing the spectral quasi-linearisation method (SQLM), was applied on these transformed equation and bounday conditions. The impact of various parameters was systematically examined and graphically presented to validate our proposed model.

2. Governing Equations

This study investigates the flow of an incompressible nanofluid in a rotating vertical cone within a magnetic field using thermal radiation as well as chemical reactions. The analysis considers thermal Biot numbers and solutal Biot numbers as borderline cases.

The physical geometry of our model is represented graphically in Figure 1. In the model, both the nanofluid and the cone rotate vertically in a particular direction with a time-dependent angular velocity (Ω). This rotation causes unsteadiness in the nanofluid. Additionally, the magnetic field is functional towards the z direction, which is the normal direction. The small magnetic Reynolds number allows for a negligible magnetic field.

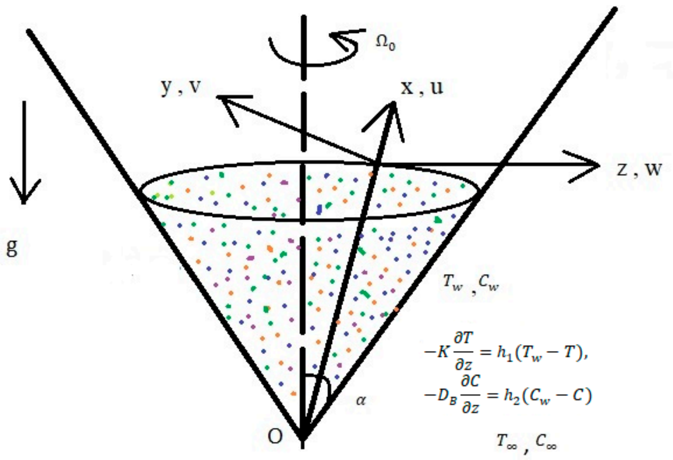

Figure 1. Physical representation of the graph.

The governing equations of our model assume thermal radiation, the presence of nanoparticles, magnetic fields, as well as chemical reactions. Borderline conditions are set using thermal and solutal Biot numbers, with reference to Takhar et al. [27] and Nadeem and Saleem [28]. These equations can be written as:

The continuity equation is:

$$\frac{\partial u}{\partial x} + \frac{u}{x} + \frac{\partial w}{\partial z} = 0, \tag{1}$$

The momentum equations are:

$$\frac{\partial u}{\partial t} + u\frac{\partial u}{\partial x} + w\frac{\partial u}{\partial z} - \frac{v^2}{x} = \nu\frac{\partial^2 u}{\partial z^2} + g\beta cos\alpha(T - T_\infty) + g\beta cos\alpha(C - C_\infty) - \frac{\sigma B^2}{\rho}u, \tag{2}$$

$$\frac{\partial v}{\partial t} + u\frac{\partial v}{\partial x} + w\frac{\partial v}{\partial z} + \frac{uv}{x} = \nu\frac{\partial^2 u}{\partial z^2} - \frac{\sigma B^2}{\rho}, \tag{3}$$

The energy equation is:

$$\frac{\partial T}{\partial t}+u\frac{\partial T}{\partial x}+w\frac{\partial T}{\partial z}=\frac{\nu}{Pr}\frac{\partial^2 T}{\partial z^2}-\frac{1}{\rho c_p}\frac{\partial q_r}{\partial z}+\tau\left(D_B\frac{\partial C}{\partial z}\frac{\partial T}{\partial z}+\frac{D_T}{T_\infty}\left(\frac{\partial T}{\partial z}\right)^2\right), \tag{4}$$

The concentration equation is:

$$\frac{\partial C}{\partial t}+u\frac{\partial C}{\partial x}+w\frac{\partial C}{\partial z}=D_B\frac{\partial^2 C}{\partial z^2}+\frac{D_T}{T_\infty}\frac{\partial^2 T}{\partial z^2}-R(C-C_\infty), \tag{5}$$

In these equations, u, v, and w represent the velocity constituents in the x (tangential), y (circumferential), and z (normal) directions, respectively. In addition, ρ is the fluid density, $\nu=\frac{\mu}{\rho}$ is the kinematic viscosity, B^2 is the uniform magnetic field, σ is the electrical conductivity, K is the thermal conductivity, q_r is the radiative heat flux, T is the temperature of the fluid, C is the concentration of the fluid, c_p is the specific heat, g is the gravitational acceleration, and β is the concentration variation constant following volumetric expansion. α is the semi-vertical approach used for the funnel. The nanoparticle heat capacity is denoted as ρc_p. The Brownian diffusion coefficient and thermophoretic diffusion coefficients are denoted as D_B and D_T, respectively.

The surface boundary conditions are non-slip, while the initial boundary conditions are determined by the ambient conditions far away from the surface.

$$u\ (x,0,\ t)=w(x,0,\ t)=0,\ v\ (x,0,t)=(\Omega_0 sin\alpha)x\psi(t^*), \tag{6}$$

$$-K\frac{\partial T}{\partial z}=h_1(T_{\ w}-T),-D_B\frac{\partial C}{\partial z}=h_2(C_{\ w}-C)\ at\ z=0,$$
$$u\ (x,\infty,\ t)=v(x,\infty,\ t)=0,\ T(x,\infty,\ t)=T_\infty,\ C(x,\infty,\ t)=C_\infty\ ,$$
$$u\ (\infty,z,\ t)=v(\infty,\ z,t)=0,\ T(\infty,z,\ t)=T_{\infty,}\ C(\infty,\ z,t)=C_\infty\ ,\ z>0 \tag{7}$$

Here, Ω_0 represents the angular velocity of the cone. Dimensional and non-dimensional times are denoted as t and t^* , respectively. The subscripts $i, wand\infty$ indicate the initial, wall, and ambient conditions, respectively.

The radiative term used in Equation (4) is calculated by employing the Rosseland approximation:

$$q_r=-\frac{4\sigma^*}{3k_1}\frac{\partial T^4}{\partial z}, \tag{8}$$

where the Stefan–Boltzmann constant is represented by σ^*, while the mean absorption coefficient is k_1.

By using Taylor's series and avoiding higher-order terms, we can accurately calculate tiny temperature differences.

$$T^4\cong 4T_\infty^3 T-3T_\infty^4, \tag{9}$$

where T_∞ is the temperature at ambient conditions.

The suitable similarity transformations are:

$$\eta=z\left(\frac{\Omega_0 sin\alpha}{\nu}\right)^{\frac{1}{2}},\ t^*=\Omega_0 sin\alpha\ t\ ,$$

$$u(x,z,t)=-\frac{1}{2}(\Omega_0 sin\alpha)H'(\eta,t^*)\psi(t^*)x,$$
$$v(x,z,t)=(\Omega_0 sin\alpha)G(\eta,t^*)\psi(t^*)x,$$
$$T(x,z,t)=T_\infty+(T_w-T_\infty)\theta(\eta,t^*)\ ,\ T_w-T_\infty=(T_{\ 0}-T_\infty)\frac{x}{L}\psi(t^*),$$
$$T(x,z,t)=T_\infty+(T_{\ 0}-T_\infty)\frac{x}{L}\theta(\eta,t^*)\psi(t^*),$$

$$C(x,z,t) = C_\infty + (C_w - C_\infty)\phi(\eta, t^*)\ ,\ C_w - C_\infty = (C_0 - C_\infty)\frac{x}{L}\psi(t^*)$$

$$C(x,z,t) = C_\infty + (C_0 - C_\infty)\frac{x}{L}\phi(\eta, t^*)\psi(t^*)$$

$$w(x,z,t) = \sqrt{\nu\Omega_0 sin\alpha}\, H(\eta, t^*)\psi(t^*) \tag{10}$$

By using the above transformations with wall temperature T_w and concentration C_w at time $t^* = 0$, the boundary conditions from Equation (7) transform into:

$$H(0,t^*) = \mathrm{H}'(0,t^*) = 0, \mathrm{G}(0,t^*) = 1,$$

$$\theta'(0,t^*) = -\mathrm{Bit}\{1 - \theta(0,t^*)\},\ \phi'(0,t^*) = -\mathrm{Bic}\{1 - \phi(0,t^*)\},$$

$$H'(\infty,t^*) = \mathrm{G}(\infty,t^*) = \theta(\infty,t^*) = \phi(\infty,t^*) \to 0, \tag{11}$$

The continuity equation (Equation (1)) was identically satisfied by these values, and we successfully converted the other equations (Equations (2)–(5)) as the steady-state equations at $t^* = 0$ by substituting $\psi = 1$, $\frac{\partial\psi}{\partial t^*} = \frac{\partial H}{\partial t^*} = \frac{\partial G}{\partial t^*} = 0$.

The transformed equations with boundary conditions as determined by governing equations are:

$$H''' - HH'' + \frac{1}{2}H'^2 - 2\mathrm{G}^2 - 2\lambda_1\theta - 2\lambda_2\phi - \mathrm{MH}' = 0, \tag{12}$$

$$G''' - (\mathrm{HG}' - \mathrm{H}'\mathrm{G}) - \mathrm{MG} = 0, \tag{13}$$

$$\frac{1}{pr}\left(1 + \frac{4}{3}R_d\right)\theta'' - \left(H\theta' - \frac{1}{2}H'\theta\right) + \mathrm{Nb}\theta'\phi' + Nt\theta'^2 = 0, \tag{14}$$

$$\phi'' - Le\left(H\phi' - \frac{1}{2}\phi H'\right) + LeR_1\phi + \frac{Nt}{Nb}\theta'' = 0, \tag{15}$$

The transformed borderline circumstances are:

$$H(0) = H'(0) = 0, \mathrm{G}(0) = 1,\ \theta'(0) = -\mathrm{Bit}\{1 - \theta(0)\},$$

$$\phi'(0) = -\mathrm{Bic}\{1 - \phi(0)\},$$

$$H'(\infty) = G(\infty) = \theta(\infty) = \phi(\infty) = 0, \tag{16}$$

where the parameters in Equations (12)–(15) are considered to be the dimension-less magnetic parameter $M = \frac{H_a}{Re_L} = \frac{\sigma \boldsymbol{B}^2}{\rho\Omega_0 sin\alpha}$ and the Hartmann number $H_a = \frac{\sigma \boldsymbol{B}^2 L^2}{\mu}$, where μ is the coefficient of viscosity, L is the characteristic length, and $Re_L = \frac{\Omega_0 sin\alpha L^2}{\nu}$ is the Reynolds number.

$Gr_1 = \frac{g\beta cos\alpha(T_w - T_\infty)L^3}{\nu^2}$ is the thermal Grashof number and $Gr_2 = \frac{g\beta cos\alpha(C_w - C_\infty)L^3}{\nu^2}$ is the mass Grashof number. The non-dimensional buoyancy force parameters are defined as $\lambda_1 = \frac{Gr_1}{{Re_L}^2}$ and $\lambda_2 = \frac{Gr_2}{{Re_L}^2}$.

$R_d == \frac{4\sigma^* T_\infty^3}{k_1 K}$ is the radiation parameter,

$Pr = \frac{\mu c_p}{K} = \frac{\nu\rho c_p}{K}$ is the Prandtl number,

$Nb = \frac{\tau D_B(C_w - C_\infty)}{\nu\rho c_p}$ is the Brownian motion parameter, $Nt = \frac{\tau D_T(T_w - T_\infty)}{T_\infty \nu\rho c_p}$ is the thermophoresis parameter,

$R_1 = \frac{R}{\Omega_0 sin\alpha}$ is the chemical reaction parameter, and

$Le = \frac{\nu}{D_B}$ is the Lewis number.

The extent of physical concern in the discussed prototypical is shown by the local skin friction coefficients, the local Nusselt number, and the local Sherwood number.

The drag function coefficients C_{fx} and C_{fy} are applied in the x and y directions, respectively:

$$C_{fx} = \frac{2\mu}{\rho(\Omega_0 x sin\alpha)^2}\left[\frac{\partial u}{\partial z}\right]_{z=0} = -Re_x^{-1/2}\psi(t^*)\mathrm{H}''(0,t^*),$$

$$C_{fy} = -\frac{2\mu}{\rho(\Omega_0 x sin\alpha)^2}\left[\frac{\partial v}{\partial z}\right]_{z=0} = -Re_x^{-1/2}\psi(t^*)\mathrm{G}'^{(0,t^*)}, \tag{17}$$

The local Nusselt number Nu_x is applied in the x direction:

$$Nu_x = -\frac{x}{T_w - T_\infty}\left(\frac{\partial T}{\partial z}\right)_{z=0} = -Re_x^{1/2}\psi(t^*)\theta(0,t^*) \tag{18}$$

The local Sherwood number Sh_x is applied in the x direction:

$$Sh_x = -\frac{x}{C_w - C_\infty}D_B\left(\frac{\partial C}{\partial z}\right)_{z=0} = -Re_x^{1/2}\psi(t^*)\phi(0,t^*) \tag{19}$$

These can be rewritten as:

$$\begin{aligned} C_{fx}Re_x^{-1/2} &= -\,\mathrm{H}''(0), \\ C_{fy}Re_x^{-1/2} &= -\,\mathrm{G}'(0), \\ Nu_x Re_x^{-1/2} &= -\left(1 + \frac{4}{3}R_d\right)\theta'(0), \\ h_x Re_x^{-1/2} &= -\,\phi'(0). \end{aligned} \tag{20}$$

3. Results and Discussion

In this investigation, we analysed a system of ODEs that were numerically solved after considering the borderline conditions with governing momentum (Equation (14)), energy, and concentration (Equations (11)–(13)). We used the spectral quasi-linearisation technique with MATLAB to analyse these equations and generate graphs for the tangential, circumferential, temperature, and solutal profiles of the parameters used in this study. The graphs provide a clear visual representation of the parameters which we will discuss in further detail.

Table 1 depicts that our solutions are in good agreement with the HAM method results reported by Nadeem and Saleem [28] in the absence of other parameters.

Table 1. Comparison of skin friction coefficients with Nadeem and Saleem [28].

λ_1	λ_2	M	$C_{fx}Re_x^{1/2}$	$C_{fy}Re_x^{1/2}$	$C_{fx}Re_x^{1/2}$	$C_{fy}Re_x^{1/2}$
			Nadeem and Saleem [28] (HAM)		Present Results (SQLM)	
1	1	1	1.93701	0.352519	1.938892	0.353567

The graphs shown below in Figure 2 demonstrate how the swiftness, heat, and solutal gradient affect the different aspects of the magnetic field parameter. For larger values of M, the tangential velocity component along the x axis initially increased for the range $0 < \eta < 4$ and then did the opposite for the range $\eta \geq 4$. On the other hand, the circumferential velocity towards the y axis and the solutal profiles decreased with a growing value of M. The magnetic field parameter, relating to Lorentz force, lead to higher resistive forces as its value increased, causing a reduction in the velocity profile. The temperature profile, on the other hand, initially decreased for the range $0 < \eta < 5$ and then increased for the range $\eta \geq 5$ as the power of the magnetic field strengthens the elements inside it at lower temperatures. Thus, the temperature profile deceased due to the buoyancy force.

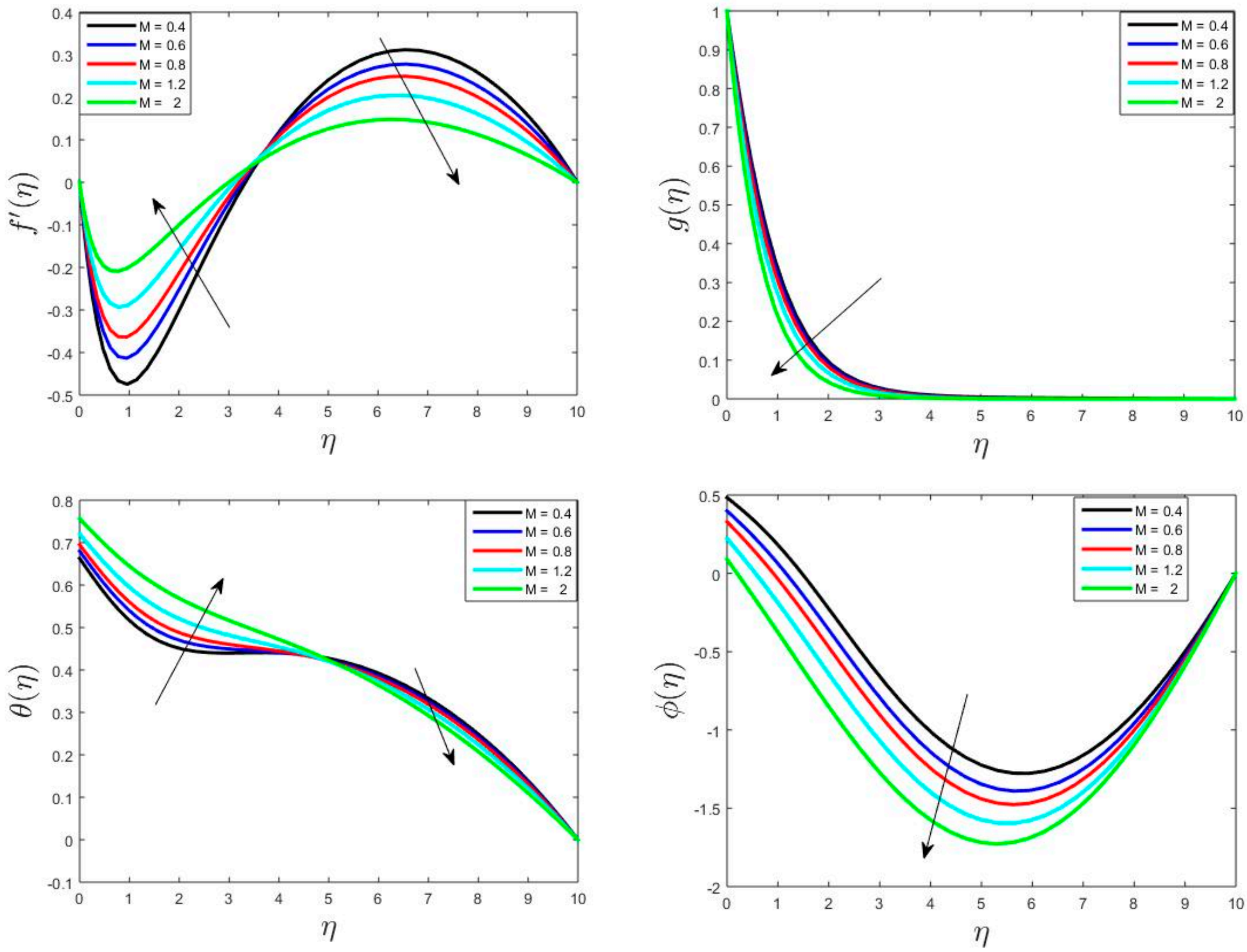

Figure 2. Influence of the magnetic parameter (M).

In Figure 3, this coefficient of Brownian motion (Nb) was found to affect the velocity component along the x axis, temperature, and solutal variation. For the range $0 < \eta < 4$, there was a higher tangential velocity and temperature distribution, while the opposite occurred for the range $\eta \geq 4$, resulting in an improved Brownian motion. As a consequence, the boundaries of the thermal layer were found to mature and thicken. This enhanced Brownian motion resulted in the increased movement of fluid particles, leading to a higher output of heat and better heat distribution. The solutal profile, on the other hand, showed the opposite trend, with a decrease in the range $0 < \eta < 4$ and a change in nature for the range $\eta \geq 4$.

Figure 4 demonstrates how the thermo-phoresis parameter Nt affects the velocity, heat, and solutal gradient. A higher Nt was found to result in a wider thermal boundary layer and dominant heat profile behaviour. This enhanced the liquefied heat profile, which in turn increased the Nt parameter. As a result, the fluids' velocity contour decreased in the range $0 < \eta < 4$ and then did the opposite for the range $\eta \geq 4$, while the solutal profile reflected a decrease in nature for the accumulated prices of the parameter.

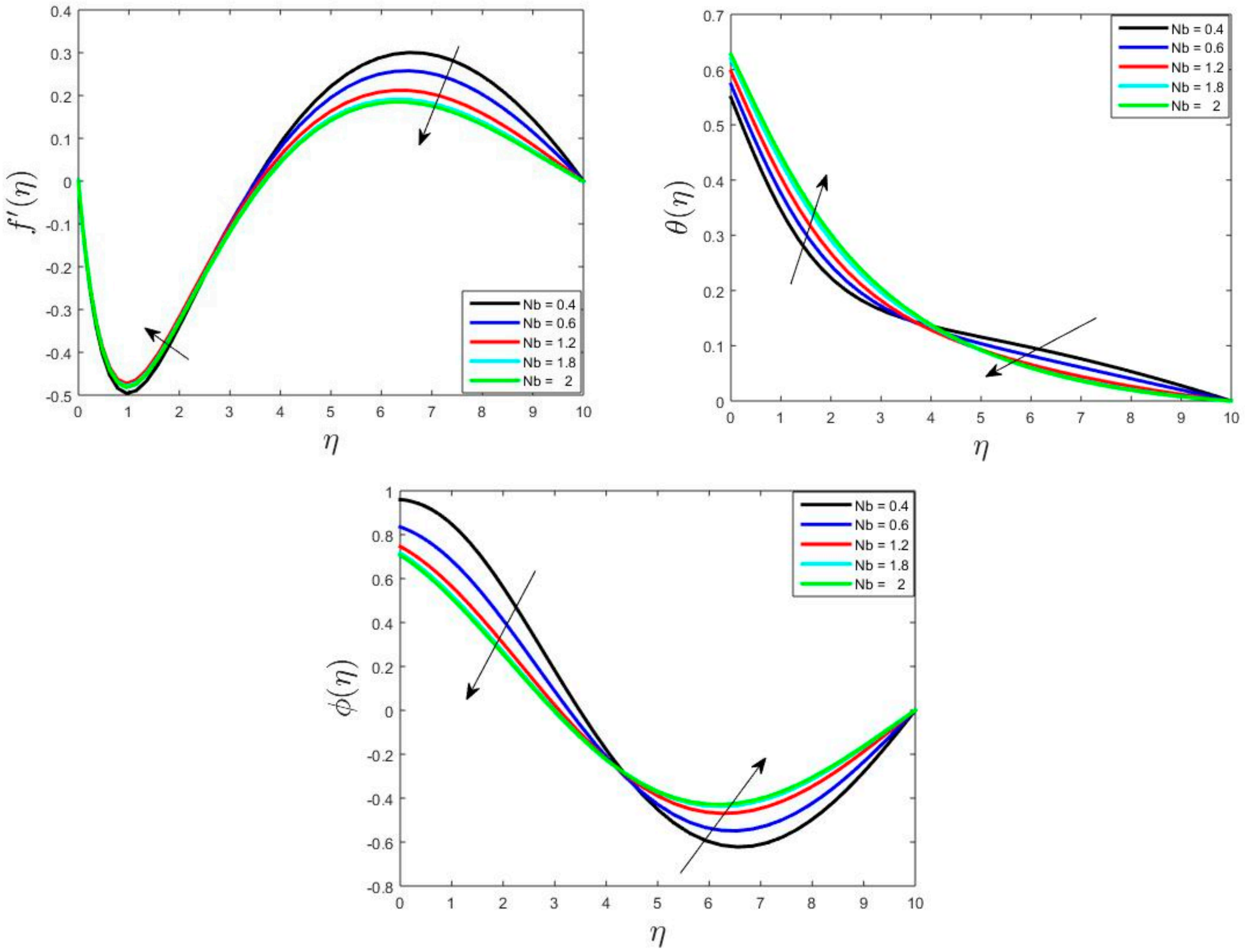

Figure 3. Impact of Brownian motion parameter (Nb).

Figure 5 displays the impact of the thermal buoyancy parameter λ_1. The graph indicates that the parameter initially favoured the tangential pace contour for the range of $0 < \eta < 3$, but then did the opposite for the range $\eta \geq 3$. Additionally, as the parameter increased and the solutal profile increased, while the circumferential swiftness and heat profiles decreased.

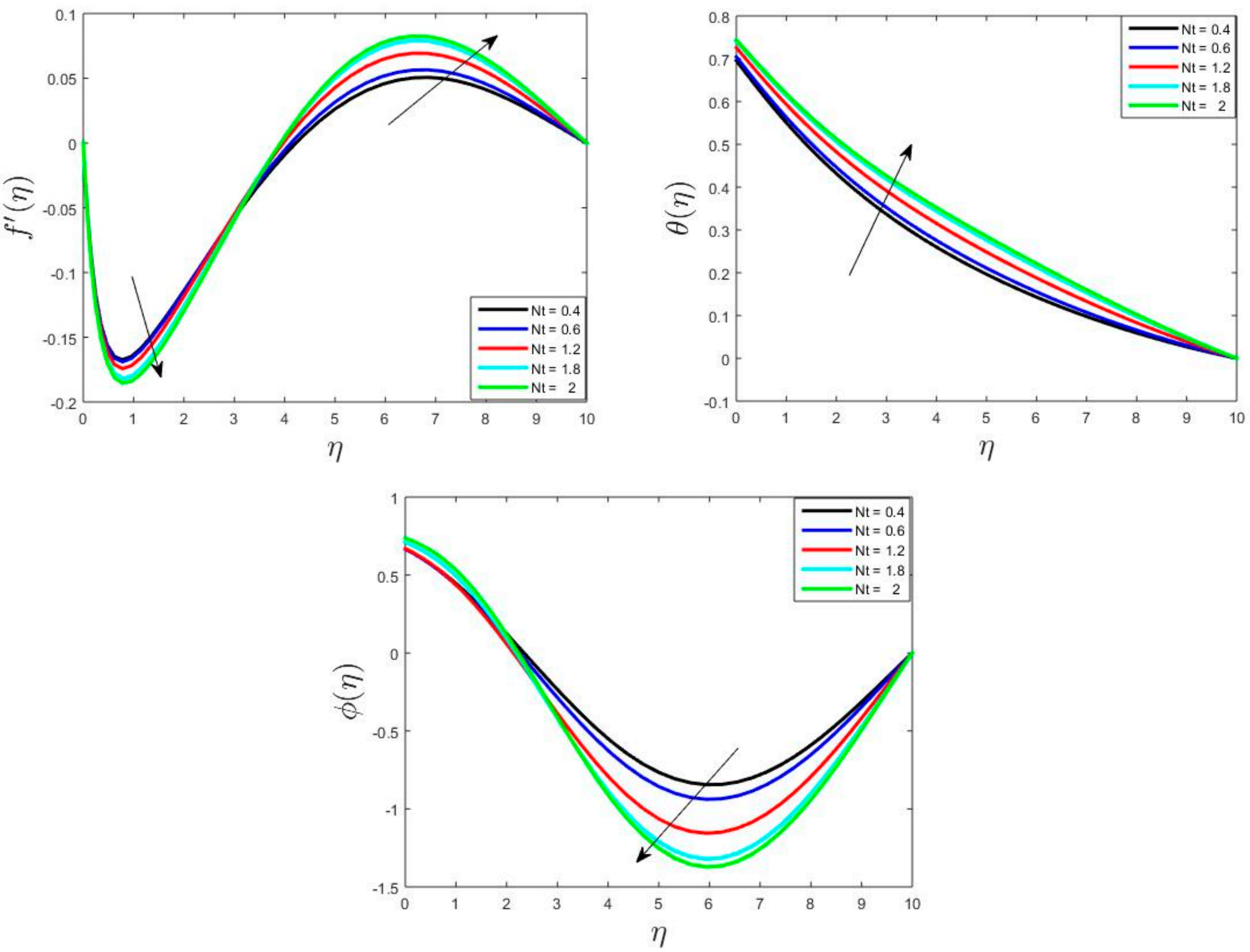

Figure 4. Impact of thermophoresis parameter (Nt).

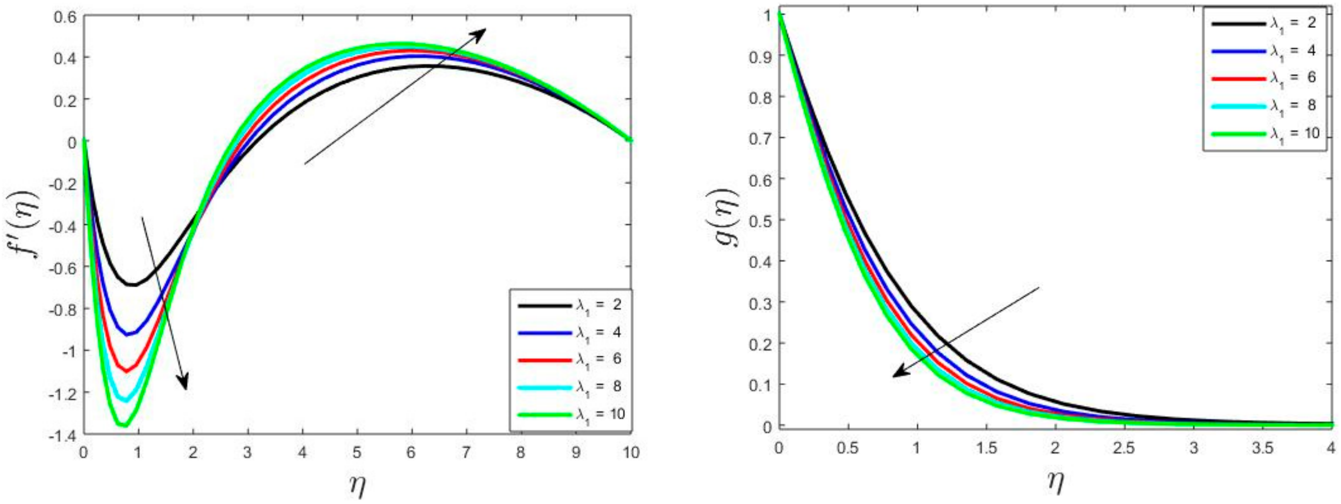

Figure 5. *Cont*.

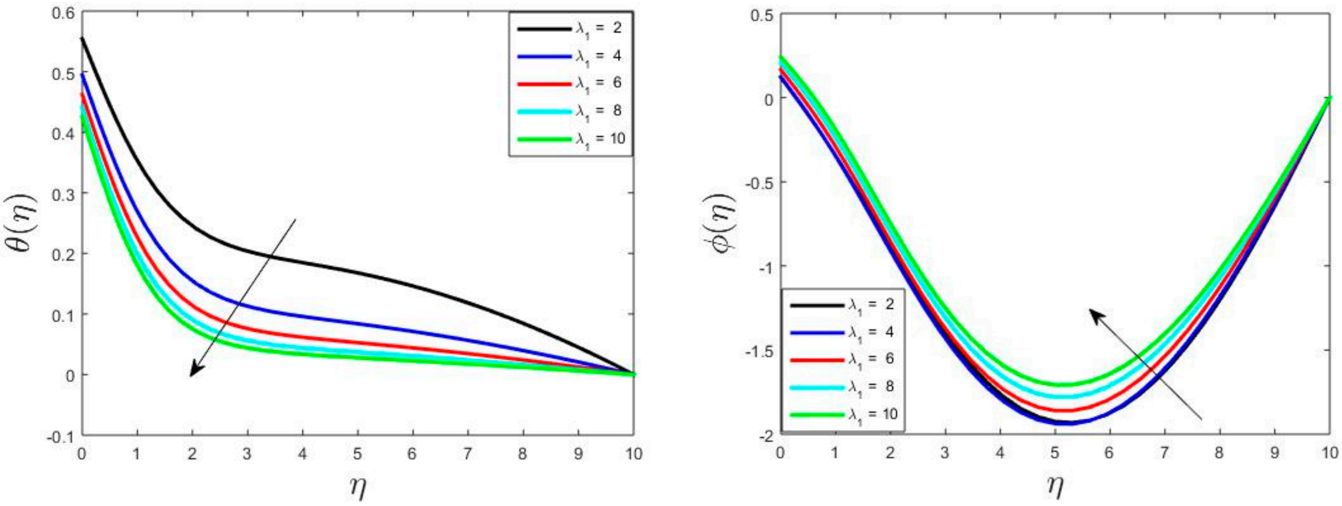

Figure 5. Impact of thermal buoyancy parameter (λ_1).

In Figure 6, the behaviour of the solutal buoyancy parameter λ_2 was highlighted. The parameter shows that the tangential pace contour initially favoured the range of $0 < \eta < 2$, but then did the opposite for the range $\eta \geq 2$. Meanwhile, the circumferential swiftness, heat, and solutal contours decreased for the accumulative values of the parameter.

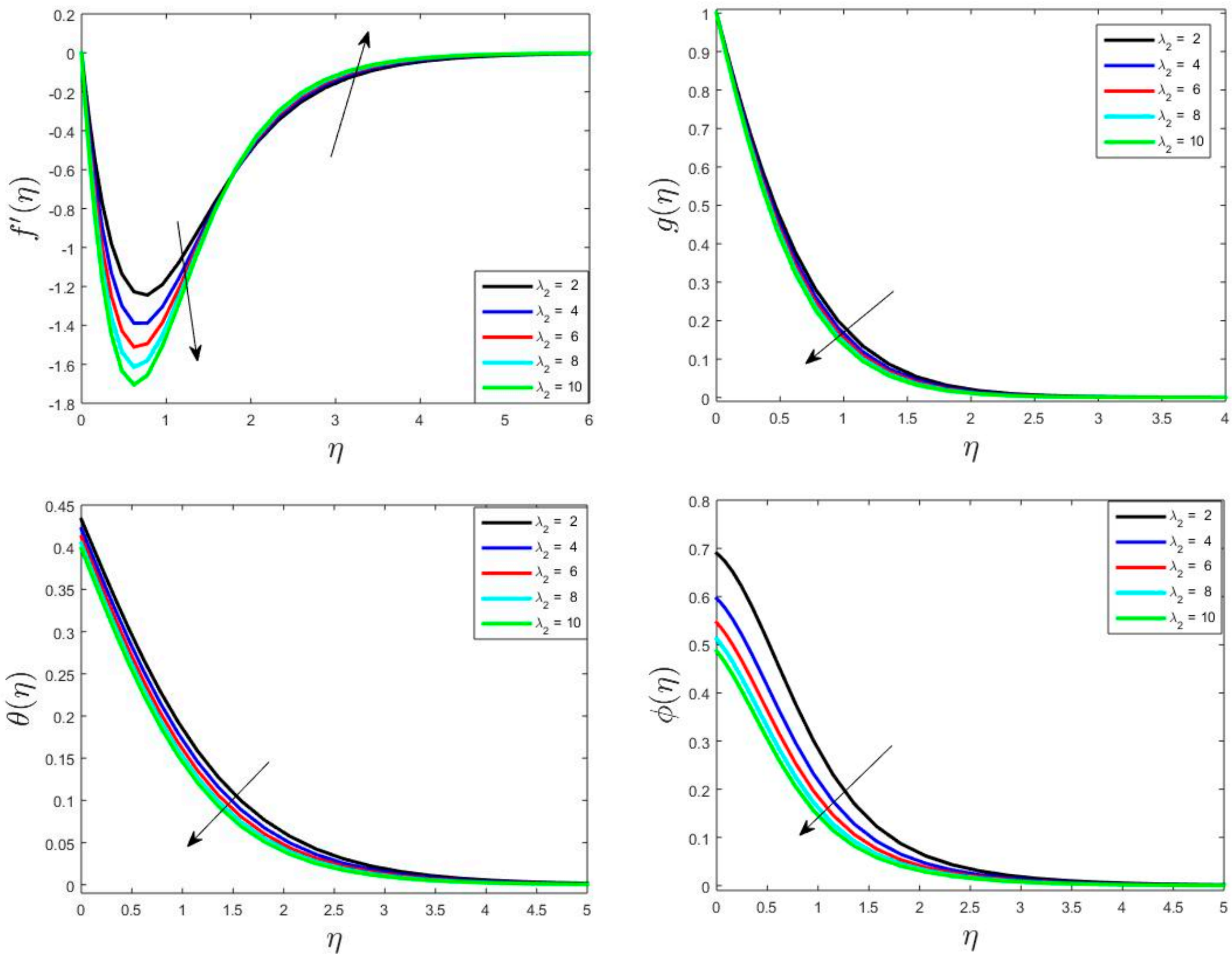

Figure 6. Impact of solutal buoyancy parameter (λ_2).

Figure 7 reflects the impact of the thermal Biot number (Bit) on velocity, heat, and concentration contours. An enhanced initial condition led to a decrease in the tangential velocity profile for the range of $0 < \eta < 4$, which then did the opposite for the range $\eta \geq 4$ while also enhancing the temperature profile and decreasing the fluid's solutal profiles.

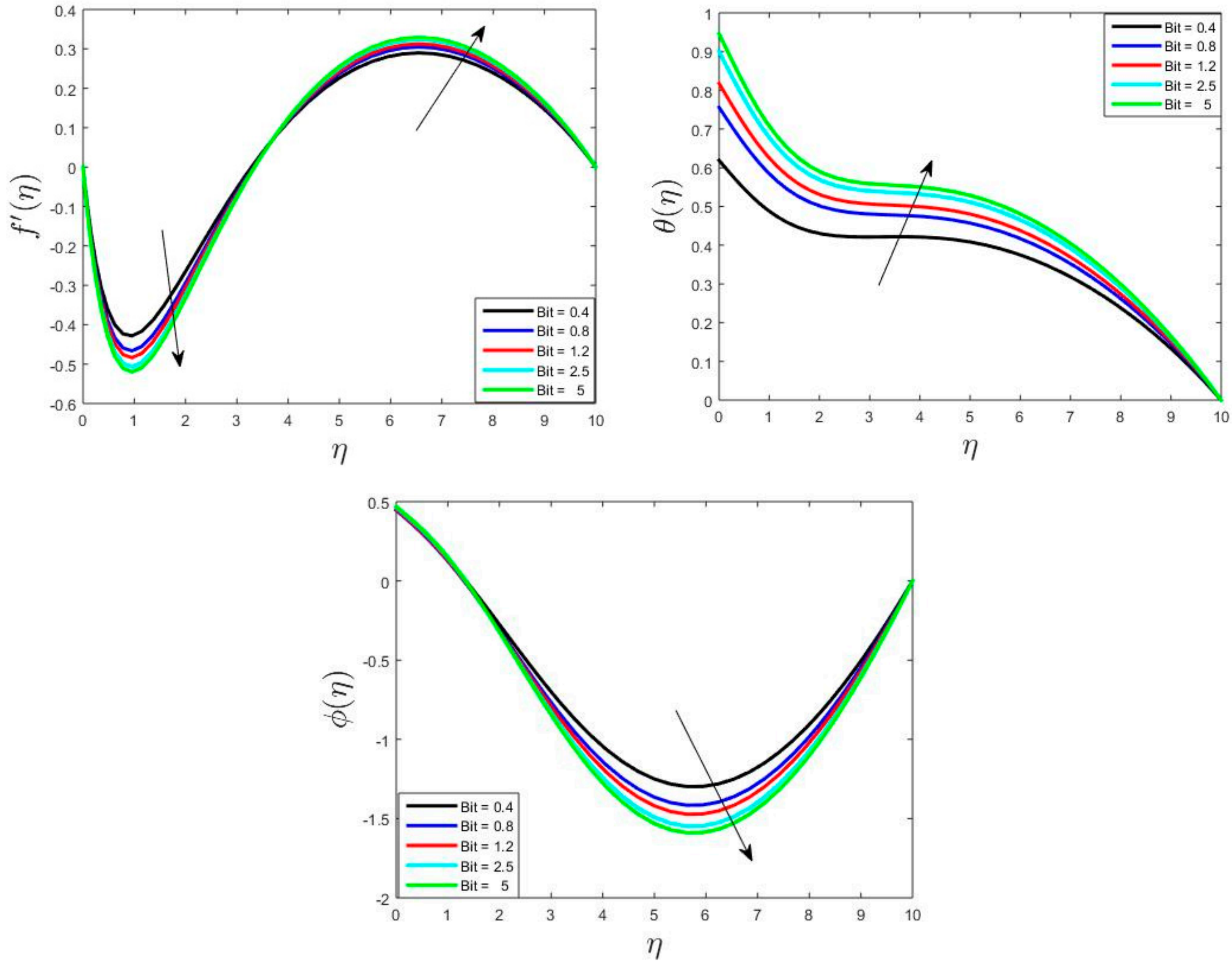

Figure 7. Impact of thermal Biot number (Bit).

The graphs in Figure 8 show how the Biot number of species (Bic) affected the velocity, heat, and concentration profiles. As the constraint increased, the heat contour increased and the solutal profile also increased for the range of $0 < \eta < 3$, but then did the opposite for the range $\eta \geq 3$. The tangential velocity of the fluid initially deceased for the range of $0 < \eta < 4$, but then did the opposite for the range $\eta \geq 4$.

The accuracy of the assumed model was confirmed by the error graph. The graph shows the norm of residual errors on the y axis and the number of iterations on the x axis. The graph provides a numerical analysis of the model's convergence and accuracy. After seven iterations, the norm of residual errors for tangential and circumferential flow, as well as others, ranged from 10^{-3} to 10^{-5}.

The results from the error graph suggest that SQLM is a suitable scheme for solving the borderline value problem. Figure 9 illustrates the norm of residual errors of the model's existing variables at various iterations.

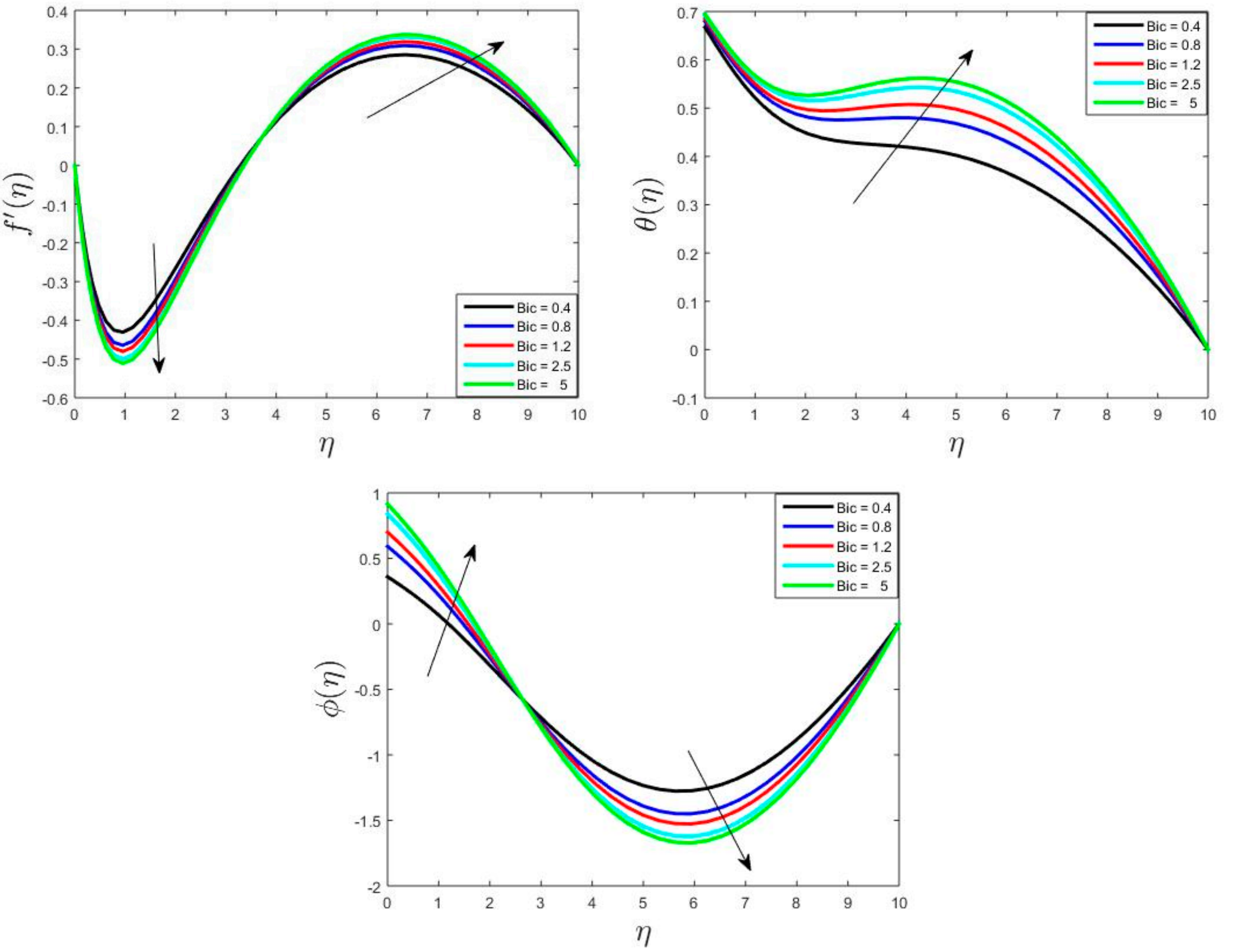

Figure 8. Influence of solutal Biot number (Bic).

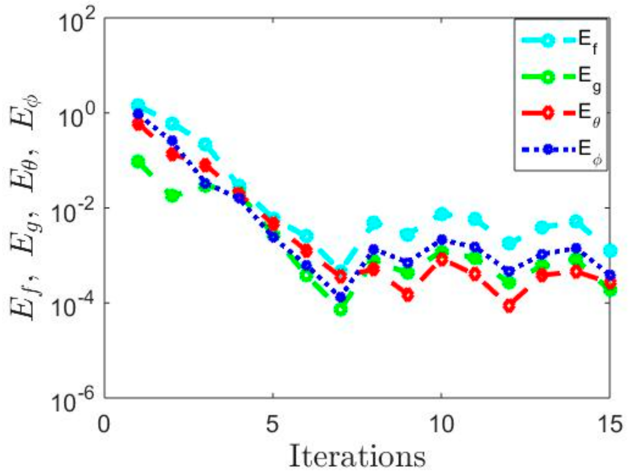

Figure 9. Error norms at different iterations.

4. Conclusions

This study aimed to analyse the unstable mixed convection nanofluid flow on a rotating vertical cone. The impact of thermal and solutal Biot numbers was examined in conjunction with the heat flux, magnetic field, chemical reaction, and thermal radiation.

The study also looked at the primary and subordinate pace, heat, and solutal contours, and analysed the impact of various parameters. MATLAB was utilised to generate the results, which were outlined as follows:

- ➢ Increase of temperature by 40% by increasing Nb from 0.4 to 2, also reflects slower movement with more solute effect.
- ➢ Improving the thermophoresis parameter (Nt) leads to an increase in velocity and temperature, but a decrease in solutal parameters.
- ➢ A higher thermal buoyancy parameter λ_1 decreases the non-dimensional circumferential flow and temperature profile.
- ➢ Enhancing thermal buoyancy parameter λ_1 increases the dimensionless tangential swiftness and solutal profiles.
- ➢ The growing standards of the solutal buoyancy parameter λ_2 discriminates the circumferential speed, temperature, and solutal profile.
- ➢ Increasing the thermal Biot coefficient (Bit) enhances the heat profile while decreasing the solutal profile of the fluid.
- ➢ Improving the solutal Biot coefficient (Bic) enhances the temperature outline while decreasing the fluid's solute profile.

Author Contributions: Conceptualization, S.M. and H.M.; Methodology, S.M. and H.M.; Formal analysis, R.B.; Writing—original draft, S.M. and H.M.; Writing—review & editing, H.M., R.B. and M.S.; Visualization, R.B. and M.S.; Supervision, H.M. All authors have read and agreed to the published version of the manuscript.

Funding: This research received no external funding.

Data Availability Statement: Data are contained within the article.

Conflicts of Interest: On behalf of all the authors, the corresponding author states that there are no competing interests regarding the research, authorship, and publication of this article.

References

1. Chamkha, A.J.; Khaled, A.R.A. Similarity solutions for hydromagnetic mixed convection heat and mass transfer for Hiemenz flow through porous media. *Int. J. Numer. Methods Heat Fluid Flow* **2000**, *10*, 94. [CrossRef]
2. Abolbashari, M.H.; Freidoonimehr, N.; Nazari, F.; Rashidi, M.M. Analytical Modelling of Entropy Generation for Casson Nano-fluid Flow Induced by a Stretching Surface. *Adv. Powder Technol.* **2015**, *26*, 542–552. [CrossRef]
3. Mishra, S.; Mondal, H.; Kundu, P.K. Analysis of Activation Energy and Microbial Activity on Couple Stressed Nanofluid with Heat Generation. *Int. J. Ambient Energy* **2024**, *45*, 2266429. [CrossRef]
4. Al-Rashed, A.A.; Kalidasan, K.; Kolsi, L.; Velkennedy, R.; Aydi, A.; Hussein, A.K.; Malekshah, E.H. Mixed Convection and Entropy Generation in a Nanofluid Filled Cubical Open Cavity with a Central Isothermal Block. *Int. J. Mech. Sci.* **2018**, *135*, 362–375. [CrossRef]
5. Manjunatha, G.; Rajashekhar, C.; Vaidya, H.; Prasad, K.V.; Saraswati; Divya, B.B. Heat transfer analysis on peristaltic transport of a jeffery fluid in an inclined elastic tube with porous walls. *Int. J. Thermofluid Sci. Technol.* **2020**, *7*, 20070101. [CrossRef]
6. Dhlamini, M.; Mondal, H.; Sibanda, P.; Motsa, S. Activation energy and entropy generation in viscous nanofluid with higher order chemically reacting species. *Int. J. Ambient Energy* **2022**, *43*, 1495–1507. [CrossRef]
7. Mishra, S.; Mondal, H.; Kundu, P.K. Analysis of Williamson Fluid of Hydromagnetic Nanofluid Flow in the Presence of Viscous Dissipation over a Stretching Surface Under Radiative Heat Flux. *Int. J. Appl. Comput. Math.* **2023**, *9*, 58. [CrossRef]
8. Dhlamini, M.; Mondal, H.; Sibanda, P.; Motsa, S. Numerical analysis of couple stress nanofluid in temperature dependent viscosity and thermal conductivity. *Int. J. Appl. Comput. Math.* **2021**, *7*, 1–14.
9. Musa, A.; Hamid, A.; Yasir, M.; Hussain, M. Effect of nonlinear thermal radiation and melting heat transfer assessment on magneto-nanofluid through a shrinking surface. *Waves Random Complex Media* **2022**, 1–18. [CrossRef]
10. Jayarami, K.; Madhusudhana, N.P.; Ramakrishna, K.; Abhishek, D. Effect of non-uniform heat source/sink on MHD boundary layer flow and melting heat transfer of Williamson nanofluid in porous medium. *Multidiscip. Model. Mater. Struct.* **2018**, *15*, 452–472.
11. Shi, Q.-H.; Khan, M.N.; Abbas, N.; Khan, M.; Alzahrani, F. Heat and mass transfer analysis in the MHD flow of radiative Maxwell nanofluid with non-uniform heat source/sink. *Waves Random Complex Media* **2021**, 1–24. [CrossRef]
12. Thumma, T.; Mishra, S.R. Effect of nonuniform haet source/sink, and viscous and Joule dissipation on 3D Eyring—Powell nanofluid flow over a stretching sheet. *J. Comput. Des. Eng.* **2020**, *7*, 412–426.
13. Kairi, R.R. Viscosity and dispersion effects on natural convection from a vertical cone in a non-Newtonian fluid saturated porous medium. *Therm. Sci.* **2011**, *15*, 307–316. [CrossRef]

14. Nasser, I.; Duwairi, H.M. Thermal dispersion effects on convection heat transfer in porous media with viscous dissipation. *Int. J. Heat Technol.* **2016**, *34*, 207–212.
15. Bhatti, M.M.; Marin, M.; Zeeshan, A.; Ellahi, R.; Abdelsalam, S.I. Swimming of motile gyrotactic microorganisms and nanoparticles in blood flow through anisotropically tapered arteries. *Front. Phys.* **2020**, *8*, 95. [CrossRef]
16. Khashi'ie, N.S.; Arifin, N.M.; Pop, I. Non-darcy mixed convection of hybrid nanofluid with thermal dispersion along a vertical plate embedded in a porous medium. *Int. Commun. Heat Mass Transf.* **2020**, *118*, 104866. [CrossRef]
17. Aghbari, A.; Agha, H.A.; Sadaoui, D. Soret-dufour effect on mixed convection past a vertical plate in non-darcy porous medium saturated with buongiorno nanofluid in the presence of thermal dispersion. *J. Mech.* **2019**, *35*, 851–862.
18. Mondal, H.; Mishra, S.; Kundu, P.K.; Sibanda, P. Entropy generation of variable viscosity and thermal radiation on magnato nanofluid flow with dusty fluid. *J. Appl. Comput. Mech.* **2020**, *6*, 171–182.
19. Meena, O.P. Mixed convection flow over a vertical cone with double dispersion and chemical reaction effects. *Heat Transf.* **2021**, *50*, 4516–4534. [CrossRef]
20. Atashafrooz, M.; Sajjadi, H.; Delouei, A.A. Simulation of combined convective-radiative heat transfer of hybrid nanofluid flowinside an open trapezoidal enclosure considering the magnetic force impacts. *J. Magn. Magn. Mater.* **2023**, *567*, 170354. [CrossRef]
21. Sheikholeslami, M.; Sajjadi, H.; Delouei, A.A.; Atashafrooz, M.; Li, Z. Magnetic force and radiation influences on nanofluid transportation through a permeable media considering Al_2O_3 nanoparticles. *J. Therm. Anal. Calorim.* **2019**, *136*, 2477–2485. [CrossRef]
22. Rashidi, M.M.; Freidoonimehr, A.M.; Rostami, B.; Hossain, M.A. Mixed convective heat transfer for MHD viscoelastic fluid flow over a porous wedge with thermal radiation. *Adv. Mech. Eng.* **2014**, *10*, 735939. [CrossRef]
23. Makinde, O.D.; Ogulu, A. The effect of thermal radiation on the heat and mass transfer flow of a variable viscosity fluid past a vertical porous plate permeated by a transverse magnetic field. *Chem. Eng. Commun.* **2008**, *195*, 1575–1584. [CrossRef]
24. Hayat, T.; Shafiq, A.; Alsaedi, A. Effect of Joule heating and thermal radiation in flow of third-grade fluid over radiative surface. *PLoS ONE* **2014**, *9*, e83153. [CrossRef] [PubMed]
25. Motsumi, T.G.; Makinde, O.D. Effects of thermal radiation and viscous dissipation on boundary layer flow of nanofluids over a permeable moving flat plate. *Phys. Scr.* **2012**, *86*, 045003. [CrossRef]
26. Makinde, O.D. MHD mixed-convection interaction with thermal radiation and nth order chemical reaction past a vertical porous plate embedded in a porous medium. *Chem. Eng. Commun.* **2011**, *198*, 590–608. [CrossRef]
27. Takhar, H.S.; Chamkha, A.J.; Nath, G. Unsteady mixed convection flow from a rotating vertical cone with a magnetic field. *Heat Mass Transf.* **2003**, *39*, 297–304. [CrossRef]
28. Nadeem, S.; Saleem, S. Unsteady mixed convection flow of nanofluid on a rotating cone with magnetic field. *Appl. Nanosci.* **2014**, *4*, 405–414. [CrossRef]